Korean J. Chem. Eng., 39(10), 2826-2833 (2022)
DOI: 10.1007/s11814-022-1138-8

pISSN: 0256-1115
eISSN: 1975-7220

The detection of Fe (III) and ascorbic acid by fluorescence quenching and recovery of carbon dots prepared from coffee waste

Sia Won and Jongsung Kim†

Department of Chemical and Biological Engineering, Gachon University,
1342 Seongnam-daero, Seongnam-si, Gyeonggi-do 13120, Korea
(*Received 17 January 2022 • Revised 2 April 2022 • Accepted 4 April 2022*)

Abstract−Coffee waste-derived carbon dots (C-CDs) that emit blue light were synthesized via hydrothermal process. The synthesized C-CDs have a round shape with average diameter of ~3.7 nm. The C-CDs show PL emission centered at 450 nm with excitation wavelength at 360 nm. The C-CDs show promising applications as Fe^{3+} sensors in aqueous solutions by fluorescence quenching. The C-CDs exhibited strong turn-off fluorescence when trace Fe^{3+} was added to the solution. Furthermore, the C-CDs-Fe^{3+} can also be used as a turn-on sensor for the detection of ascorbic acid (AA). AA reduces Fe^{3+} to Fe^{2+}, resulting in the recovery of fluorescence intensity of the quenched C-CDs. Thus, the C-CDs can be used as a rapid and effective dual mode "off-on" fluorescence sensor for Fe^{3+} and AA. The fluorescence response exhibits a good linear relationship with the concentration of Fe^{+3} and AA in the range of 0-100 and 0-1 μM, with a limit of detection (LOD) around 4.314 and 0.162 μM, respectively.

Keywords: Coffee Waste, Carbon Dots, Biosensor, Dual-mode Fluorescence Sensor

INTRODUCTION

Carbon dots (CDs) are fluorescent materials made of carbon that have peculiar electrical and optical properties with particle size less than 10 nm [1,2]. Recently, carbon-based nanomaterials like CDs showing tunable optical bandgap features associated with the quantum confinement effect have been widely used in photo-catalysis, and energy conversion and storage fields [3-9]. Other research fields of interest for the CDs include environmental sensing [10], bioimaging [11], and drug delivery platforms for cancer [12]. In addition to their low toxicity [13] and high quantum efficiency, CDs possess interesting characteristics, such as tunable optical properties [14], ease of synthesis [15,16] and abundant surface functionalities [17,18]. Research on the development of sensors of various materials using carbon points with high luminous efficiency is actively continuing [19-23]. CDs can be synthesized using either a bottom-up or top-down approach [24,25]. In our previous studies, we prepared CDs using various natural sources, such as broccoli, corn, persimmon, onion, and curcumin for bio-sensing and bioimaging applications [26-29].

With population growth and urbanization, global wastes increase very rapidly [30]. Recently, coffee beans have become one of the most traded products in the world, and their annual consumption continuously increases, generating large amounts of coffee waste every year. Most of them are landfilled, which will eventually result in the soil pollution and various environmental problems [31]. To solve the environmental issues by coffee wastes, the alternative utilization of coffee wastes should be prepared [32]. Coffee waste is made up of various organic compounds that can be potentially converted into a variety of pollutants [33].

Several cellular functions are operated by various ions such as Fe^{3+}, Cu^{2+}, K^+, Na^+, and Cl^-, and molecules such as ascorbic acid and glutamic acid. Fe^{3+} ions play an important role in various intracellular biochemical processes, such as DNA replication, cell proliferation, oxygen transport, and enzyme catalysis [34]. Fe^{3+} deficiency or excess accumulation interferes with the biochemical processes, causing various diseases such as anemia, cancer, and organ dysfunction [35,36]. Therefore, sensitive, and accurate detection of Fe^{3+} in the body is very important [37].

AA is extensively used in the food industry [38]. AA has antioxidant properties and plays an important role in maintaining the balance of oxidative stress in many biochemical processes. It is used as a therapeutic agent for liver disease, allergic reactions, scurvy, and helps in healthy cell development, calcium absorption, and normal tissue growth [39,40]. In this report, we discuss the preparation of C-CDs from coffee wastes and applications of the C-CDs as dual sensors for Fe^{3+} and AA detection. The fluorescence quenching and recovery of C-CDs are used for sensing.

EXPERIMENTAL

1. Materials

Coffee wastes obtained from a local café in Seongnam City were used as precursors for the carbon dots. Ethyl alcohol (70-75% extra pure grade) was purchased from DAEJUNG (Republic of Korea). Hydrogen peroxide solution (30% (w/w) in H_2O), $Zn(NO_3)_2$, $Cd(NO_3)_2$, $Ba(NO_3)_2$, $Mg(NO_3)_2$, KNO_3, $Mn(NO_3)_2$, $AgNO_3$, $Pb(NO_3)_2$, $Fe(NO_3)_3$, urea, cysteine, glutamic acid, ascorbic acid, and citric acid were purchased from Sigma-Aldrich (USA). Deionized (DI) water was used in all the experiments. The dialysis membrane (MWCO

†To whom correspondence should be addressed.
E-mail: jongkim@gachon.ac.kr

of 100-500 D) was purchased from Spectrum Laboratories, Inc.

2. Instruments and Measurements

Field-emission transmission electron microscopy (FE-TEM) images were obtained using an FE-TEM (Thermal FED Type, JEM-F200 (TFEG), JEOL Ltd.) instrument. Fourier-transform infrared (FT-IR) spectra were obtained using an FT-IR spectrometer (Bruker, Vertex 70). X-ray diffraction (XRD) patterns were obtained using a high-resolution X-ray diffractometer with a high-temperature stage (Rigaku, Smartlab). X-ray photoelectron spectroscopy (XPS) data were obtained using an XPS instrument (Multilab-2000, Thermo Fischer Scientific). Ultraviolet-visible (UV-Vis) absorbance spectra were obtained using a UV-Vis spectrophotometer (Varian Cary 100). Photoluminescence (PL) emission spectra were obtained using a fluorescence spectroscopy system (Photon Technology International, FRET MASTER-1 with Remote Sensing System) at Smart Materials Research Center for IOT in Gachon University.

3. Synthesis and Purification of C-CDs

The coffee wastes were soaked in ethyl alcohol (1 : 1 mass ratio) for 1 h. The suspension was filtered using a filter paper and concentrated using a rotary evaporator at 60 °C. Thereafter, 5 mL of concentrated coffee extract and 5 mL of hydrogen peroxide were mixed in 45 mL of DI water and stirred for 5 min. The solution was sealed in a 100 mL Teflon-lined autoclave, followed by hydrothermal treatment at 180 °C for 1 h to create C-CDs. The autoclave was subsequently cooled to room temperature, and the C-CDs solution was dialyzed with a dialysis membrane for 48 h against DI water to remove the unreacted materials and impurities. Finally, the dialyzed solution was evaporated overnight at 60 °C to obtain the C-CDs powder.

4. Detection of Fe^{3+}

Various concentrations of iron solution (0-200 μM) were prepared by dissolving $Fe(NO_3)_3$ in DI water. The C-CDs solution (3 mL) was mixed with 3 mL of iron solution at different concentrations, and the PL spectra were recorded. The fluorescence quenching of the C-CDs by Fe^{3+} was observed.

For the selectivity test of Fe^{+3} over other ions, 1 mL (1 mM) of Fe^{3+} and various metal ions (Zn^{2+}, Cd^{2+}, Ba^{2+}, Mg^{2+}, K^{+}, Mn^{2+}, Ag^{+}, Pb^{2+}) were added to the C-CD solution (5 mL) and kept for 10 min. The PL emission spectra of the solutions were recorded at an excitation wavelength of 360 nm. The fluorescence quenching was then compared.

5. Detection of AA

Various concentrations of AA (0-1 μM) solutions were prepared and added to the fluorescence quenched C-CDs -Fe^{3+} (100 μM) solution and the PL spectra were recorded. The fluorescence recovery was observed due to the reduction of Fe^{+3}.

For the selectivity test, 2 mL (2 mM) of ascorbic acid and various biomolecules (citric acid, cobalamin, urea, starch, L-lysine monohydrochloride, L-glutamine, and glutamic acid) were added to the C-CD-Fe^{3+} (100 μM) solutions (2 mL) and kept for 10 min. The PL emission spectra of the solutions were recorded at an excitation wavelength of 360 nm. The fluorescence recovery was then compared.

RESULTS AND DISCUSSION

1. Characterization of CDs

Fig. 1(a) presents the TEM image and particle size distribution of the C-CDs, demonstrating that the C-CDs were well dispersed with an average size of 3.7 nm. Fig. 1(b) shows the fast Fourier-transform (FFT) pattern, indicating the (111) graphitic planes of the C-CDs [41]. The inset image reveals a lattice spacing of 2.6 Å. Fig. 2(a) shows the PL emission spectra of the C-CDs with excitation wavelength varied from 310 to 390 nm. With an increase in the excitation wavelength, the emission peak shifted from 434 to 469 nm. The PL emission maximum was observed at 450 nm, corresponding to blue emission with excitation wavelength at 360 nm. Fig. 2(b) shows the combined UV-vis absorption spectra and PL emission spectra of the C-CDs in DI water, PBS, and human serum. The absorbance and emission spectra of the C-CDs were similar in all three media, which means that the C-CDs can be used for sensing experiment both in vivo and in vitro. Fig. 2(c) shows the maximum PL intensity of C-CDs at various pH values. The C-CDs show a maximum PL intensity at pH 7. This result suggests

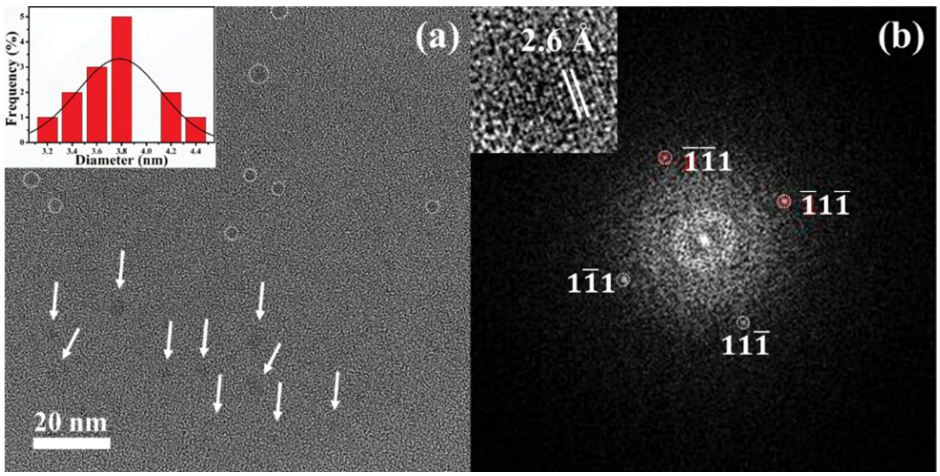

Fig. 1. (a) FE-TEM image of C-CDs; inset displays the histogram of the size distribution of C-CDs; (b) corresponding FFT pattern of C-CDs; inset displays the lattice fringes of 2.6 Å.

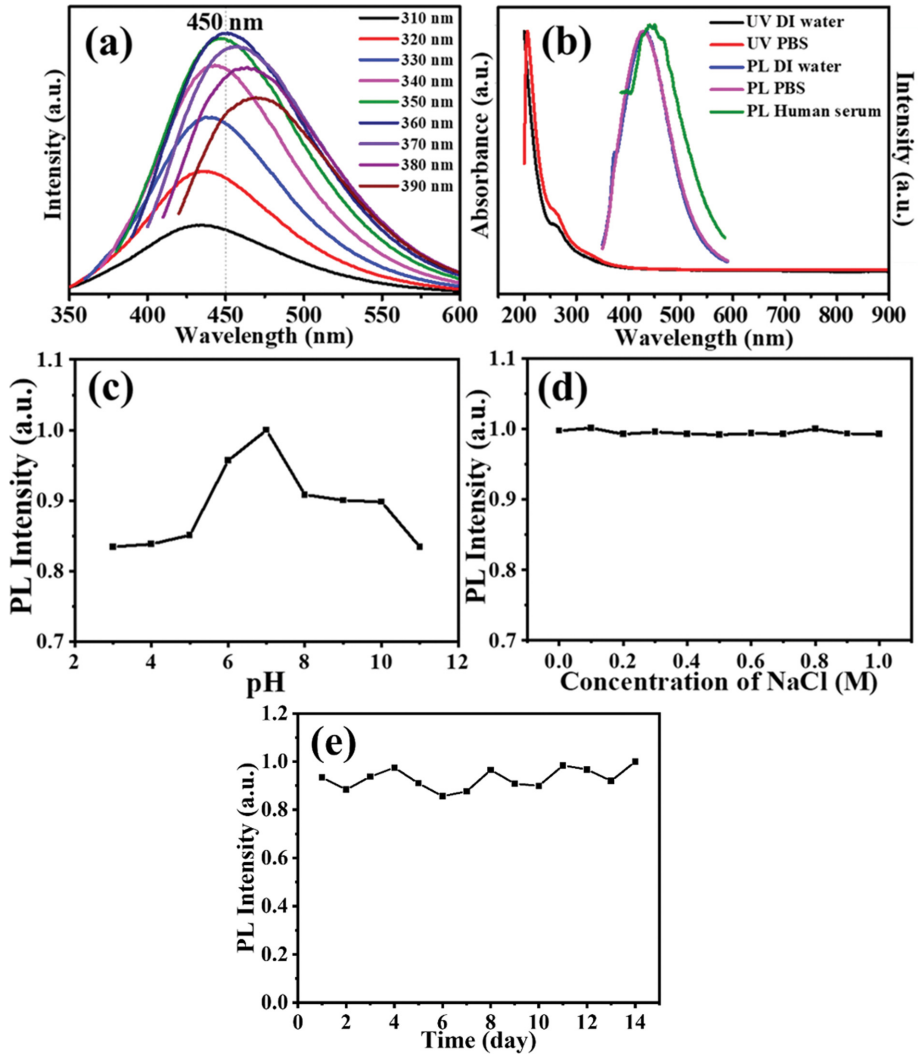

Fig. 2. (a) PL emission spectra of C-CDs with excitation wavelength varied from 310 to 390 nm; (b) UV-vis spectra and PL emission spectra with excitation at 360 nm for C-CDs in DI water, PBS buffer, and human serum; The dependence of PL intensity of C-CDs on (c) pH and (d) NaCl concentration; (e) Long-term stability of C-CDs with fluorescence at 450 nm under excitation at 320 nm.

that the PL intensity of C-CDs is dependent on pH, and following sensing experiment was performed at pH 7. Fig. 2(d) shows that NaCl concentration does not affect the PL intensity. This ensures that C-CDs can be used in physiological condition of various NaCl concentrations. The C-CDs did not display any meaningful reductions in PL intensity despite the passage of time as shown in Fig. 2(e). This indicates the excellent photostability and storage stability of C-CDs, showing their high efficiency as a sensor material. During the measurement period, C-CDs were stored and sealed at room temperature. Fig. 3. shows the high-resolution XPS data for the C-CDs. Fig. 3(a) shows a Si 2p peak at 102.1 eV, suggesting that silicon is bound in the R_2-Si-O_2 form [42], where R symbolizes carbon-and hydrogen-containing partial structures [43]. This is a bond of Si, a constituent of coffee waste [44]. The C 1s profile in Fig. 3(b) was de-convoluted into four peaks at 283.1, 284.8, 286.6, and 288.6 eV, which can be ascribed to Si-C, C-C/C-H, C-O-C, and O-C=O, respectively [45-47]. The N 1s spectrum shown in Fig. 3(c) presents two peaks, corresponding to N=C at 400.0 eV and -NH_4 at 401.9 eV [48,49]. The O 1s peak of the C-CDs could be split into five peaks, as shown in Fig. 3(d). These peaks are attributed to O-H, C=O, C-O, O=C-O, and C-OH with binding energies of 531.1, 531.4, 532.5, 533.6, and 534.5 eV, respectively [50-52]. All binding energies in the XPS graph were calibrated using the C 1s peak at 284.8 eV [53].

Fig. 4(a) presents the FT-IR spectra of the C-CDs. The peaks at 615, 1,214, 1,454, 1,714, 1,980, 2,050, 2,161, 2,348, 3,612, and 3,714 cm^{-1} are attributed to the vibrations of =C-H, C-O, -CH_4, -COOH, C=C=C, O=C=O, C≡C, -NH_4, and -OH, respectively. Furthermore, the four absorption peaks at 671, 765, 956, and 1,780 cm^{-1} are associated with the stretching and bending vibrations of -OH, C-H, C=C, and C=O, respectively [54-61]. The XPS and FT-IR data are consistent, confirming that the C-CDs have various surface functional groups. Fig. 4(b) shows the XRD pattern of the C-CDs. The broad peak at 19.16° corresponds to the (002) plane (JCPDS 26-1076) [62,63]. This XRD pattern is consistent with the TEM results for the C-CDs and reveals that the C-CDs have a graphitic struc-

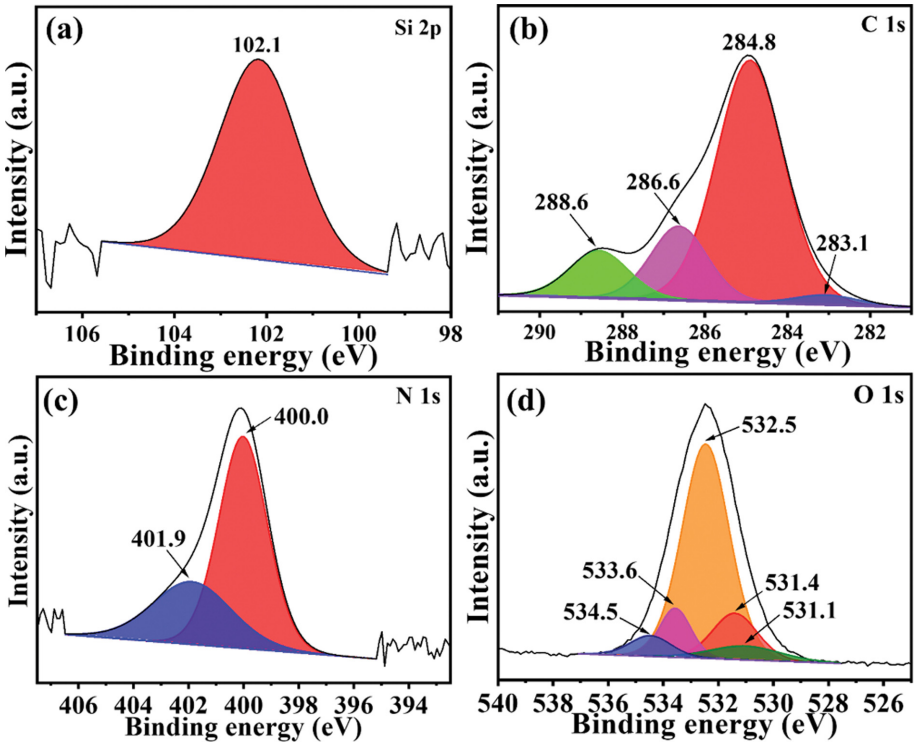

Fig. 3. High-resolution XPS spectra of (a) Si 2p. (b) C, (c) N, and (d) O for the C-CDs, respectively.

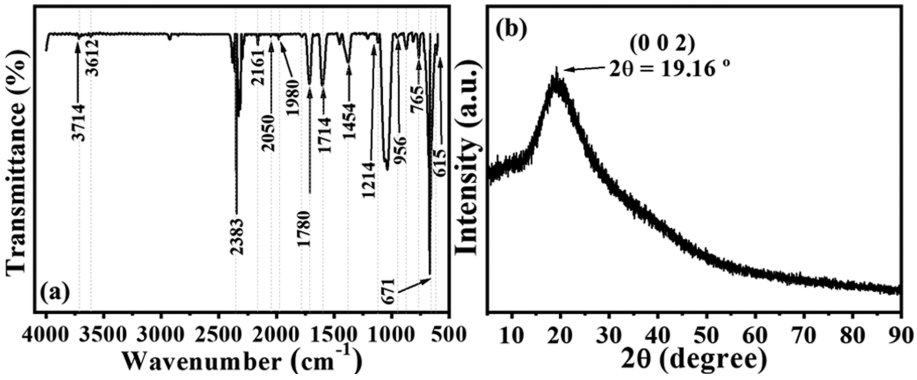

Fig. 4. (a) FT-IR spectra of C-CDs; (b) XRD pattern of C-CDs.

ture predominantly [64].

2. Sensing of Metal Ions and Biomolecules

2-1. Metal Ion Detection Using C-CDs

The selective and sensitive detection of metal ions using CDs has been reported by various research groups. CDs are used as fluorescence probes for the detection of various important analytes [65]. Changes in the fluorescence intensity of C-CDs make it possible to determine the presence or absence of a specific ion among various metal ions. Fig. 5(a) shows the PL spectra of the C-CDs with various concentrations of Fe^{3+} ions. The excitation wavelength was 360 nm, and the PL intensity at 460 nm decreased gradually as the concentration of Fe^{3+} increased. The inset shows a gradual decrease in the emission intensity. Fig. 5(b) shows the linear relationship between the PL quenching and the Fe^{3+} ion concentration. The Stern-Volmer equation [66] was used to measure the linearity of the response:

$$\frac{F_0}{F} = 1 + K_q[Fe^{3+}] \quad (1)$$

where K_q is the Stern-Volmer constant, representing the affinity between the fluorophore and quencher, and F and F_0 are the PL intensities of the C-CDs in the presence and absence of Fe^{3+} ions, respectively [67]. A very good linear relationship was observed with a correlation coefficient of R^2=0.9984 in the Fe^{3+} concentration range of 0 to 100 μM. This shows that the C-CDs can be used as Fe^{3+} sensor by fluorescence quenching. The limit of detection (LOD) was 4.314 μM and the limit of quantification (LOQ) was 13.07 μM. The LOD of the C-CDs was calculated as 3.3 (σ/s) and the LOQ was calculated as 10(σ/s), where 3.3, σ, and S represent the expansion factor, the standard deviation of the blank signal, and the

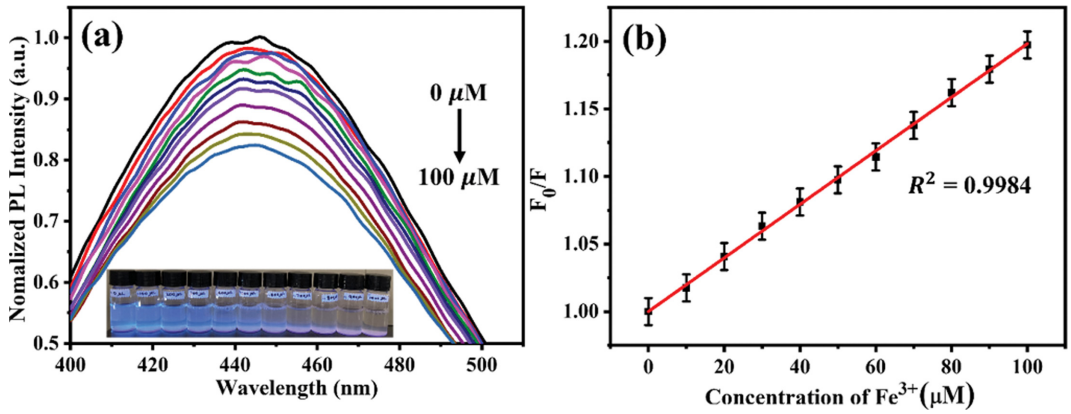

Fig. 5. (a) PL emission spectra of C-CDs with various concentrations of Fe^{3+} (0 to 100 μM); inset shows photograph of C-CDs quenched by Fe^{3+}; (b) linear relationship between PL quenching of C-CDs and concentration of Fe^{3+} ions.

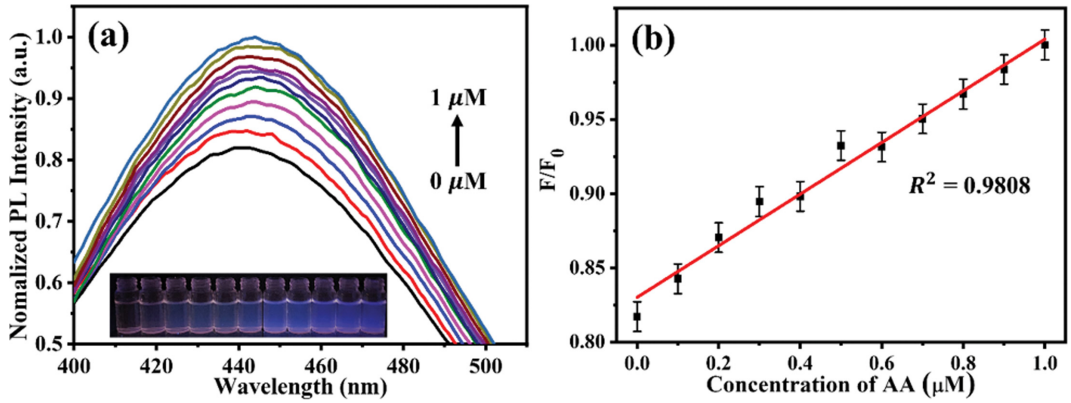

Fig. 6. (a) PL emission spectra of C-CDs-Fe^{3+} (100 μM) with increasing AA concentration from 0 to 1 μM; inset shows photograph of C-CDs-Fe^{3+} recovery by AA; (b) linear relationship of fluorescence recovery of C-CDs-Fe^{3+} vs. AA concentration.

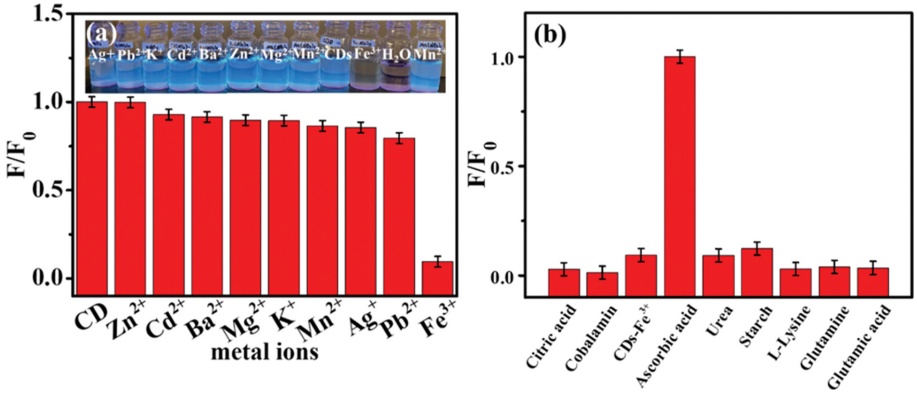

Fig. 7. (a) Selectivity of C-CDs for Fe^{3+} sensing over other metal ions; inset displays photo-graphs of C-CDs with various metal ions under UV light; (b) Selectivity of C-CDs-Fe^{3+} for ascorbic acid sensing over various biomolecules.

slope of the linear calibration plot, respectively [68,69].

2-2. Biomolecule Detection Based on CDs-Fe^{3+}

Fig. 6(a) shows the recovery of the PL intensity of the C-CDs upon the addition of AA to the C-CD-Fe^{3+} (100 μM) system. The PL intensity of C-CDs was quenched with the addition of Fe^{3+} ions, but gradually recovered with the addition of AA. As the AA concentration increased, the PL intensity steadily increased. The inset shows a gradual increase in the emission intensity. Fig. 6(b) shows the linear relationship between the PL intensity and AA concentration. The figure shows a very good linear relationship with a correlation coefficient of R^2=0.9808 in the range of 0 to 1 μM. AA can be detected by PL recovery in the C-CD-Fe^{3+} (100 μM) system with an LOD of 0.162 μM and an LOQ of 0.491 μM. This shows that the C-CD-Fe^{3+} (100 μM) system can be used as a good probe

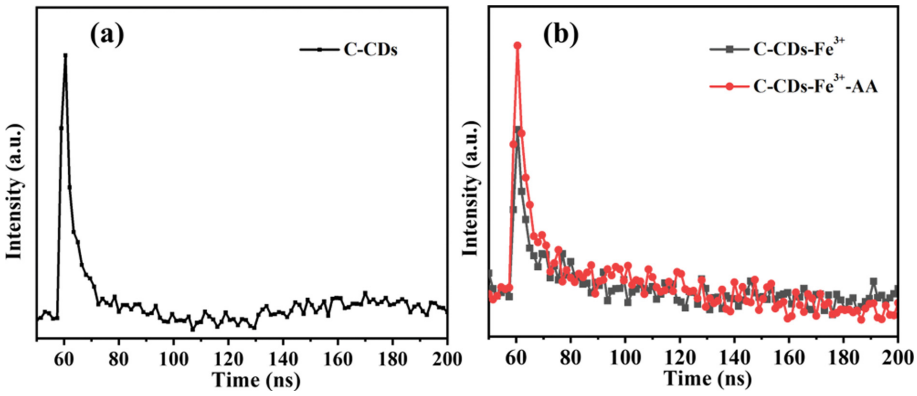

Fig. 8. (a) Fluorescence lifetime decay of (a) C-CDs and (b) C-CDs-Fe^{3+} and C-CDs-Fe^{3+}-AA.

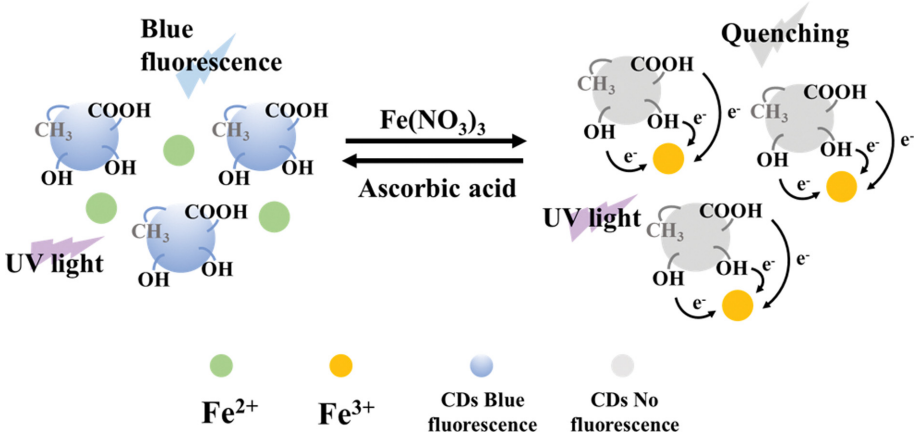

Fig. 9. Schematic of the mechanism of PL turn-on and turn-off of C-CDs with the addition of Fe^{+3} and AA.

for AA detection.

Fig. 7(a) shows the selectivity for Fe^{3+} ions over other metal ions (Cd^{2+}, Ba^{2+}, Mg^{2+}, K^{+}, Mn^{2+}, Ag^{+}, Pb^{2+}, etc.) based on PL quenching of the C-CDs. Only Fe^{3+} ions induced PL quenching of the C-CDs. The PL intensity of the C-CDs decreased to approximately 9.5% of the initial intensity. The inset shows an image of the C-CD solution containing various metal ions under UV illumination. Fig. 7(b) shows that only AA recovered fluorescence most efficiently compared with other biomolecules (Citric acid, Cobalamin, Urea, Starch, L-Lysine monohydrochloride, L-Glutamine, Glutamic acid), which means that the constructed fluorescent probe was highly selective toward ascorbic acid. The PL intensity of the C-CD-Fe^{3+} increased to approximately 10.8 times of the initial intensity. The linear range and the LOD were more significant than the recently reported ones for AA detection (see Table 1) [70-74].

The PL quenching mechanism for the C-CDs was confirmed through fluorescence lifetime decay analysis, as illustrated in Fig. 8. These decay curves were fitted via double exponential fitting according to the given equation:

$$D(t) = \Sigma_{i=1}^{n} a_i \exp\left(-\frac{t}{\tau_i}\right) \quad (2)$$

Here, D, τ_i, and ai indicate the PL decay, lifetime, and pre-exponential factors, respectively [25]. The C-CDs showed a lifetime τ_1 of 11.56 ns and lifetime τ_2 of 0.025 ns. Significantly, when Fe^{3+} ions (100 μM) were added to the C-CDs, τ_1 decreases to 8.54 ns and τ_2 0.020 ns. The C-CDs-Fe^{3+} (100 μM) was added to the AA (1 μM), resulting in the increasing the lifetime τ_1 of 12.25 ns and lifetime τ_2 of 0.028 ns.

Based on the above results, a schematic of the PL quenching and recovery mechanism is shown in Fig. 9. The C-CDs have numerous surface oxygen-containing functional groups. Fe^{3+} always prefers to bind with oxygen-containing functional groups owing to hard acid-hard base interactions. Upon binding with the oxygenous surface functional groups, electrons from the conduction band of the C-CDs can be transferred to the unfilled d-orbitals of Fe^{3+} in a rapid non-radiative manner, leading to fluorescence quenching. Therefore, through this turn-off quenching process, Fe^{3+} ions can be detected. When AA was added, Fe^{3+} was reduced to Fe^{2+}. Upon reduction of Fe^{3+} to Fe^{2+}, the generated Fe^{2+} does not prefer to bind with oxygen-containing functional groups via coordination interactions. As a result, the PL intensity can be recovered (turn-on) by the addition of AA.

CONCLUSIONS

CDs were successfully synthesized from coffee waste using a low-cost and eco-friendly process. The as-synthesized C-CDs were

utilized for the detection of Fe^{3+} and AA via "turn-off" and "turn-on" responses, respectively. The fluorescence of the C-CDs was quenched with the addition of Fe^{3+}, and a very good linear relationship was observed between the PL quenching and Fe^{3+} concentration in the range of 0 to 100 μM with LOD and LOQ values of 4.314 and 13.074 μM, respectively. The PL quenched C-CD-Fe^{3+} (100 μM) system was used as a probe to detect AA. When AA was added to the C-CD-Fe^{3+} (100 μM) system, the PL intensity of the C-CDs was recovered. AA was detected in the range of 0 to 1 μM with LOD and LOQ values of 0.162 and 0.491 μM, respectively. C-CDs can be used as Fe^{3+} and AA dual sensors with features such as fast detection speed, high sensitivity, and selectivity.

ACKNOWLEDGEMENTS

This research was supported by Basic Science Research Program through the National Research Foundation of Korea (NRF) funded by the Ministry of Education (2021R1A6A1A03038996) and by the Gachon University research fund of 2020 (GCU-202002400001).

CONFLICTS OF INTEREST

There are no conflicts to declare.

REFERENCES

1. V. A. Ansi and N. K. Renuka, *J. Lumin*., **205**, 467 (2019).
2. M. Moniruzzaman and J. Kim, *Sens. Actuators, B Chem*., **295**, 12 (2019).
3. Y. Wang and N. Herron, *J. Phys. Chem*., **95**, 525 (1991).
4. H. Li, X. He, Z. Kang, H. Huang, Y. Liu, J. Liu, S. Lian, C. H. A. Tsang, X. Yang and S.-T. Lee, *Angew. Chem*., **122**, 4532 (2010).
5. H. M. Yadav and J. S. Kim, *J. Alloys Comp*., **688**, 123 (2016).
6. K. A. S. Fernando, S. Sahu, Y. Liu, W. K. Lewis, E. A. Guliants, A. Jafariyan, P. Wang, C. E. Bunker and Y. P. Sun, *ACS Appl. Mater. Interfaces*, **7**, 8363 (2015).
7. V. C. Hoang, K. Dave and V. G. Gomes, *Nano Energy*, **66**, 104093 (2019).
8. H. M. Yadav, N. C. Deb Nath, J. Kim, S. K. Shinde, S. Ramesh, F. Hossain, I. Olaniyan and J. J. Lee, *Polymers*, **12**(8), 1666 (2020).
9. S. Mohapatra, S. Sahu, N. Sinha and S. K. Bhutia, *Analyst*, **140**, 1221 (2015).
10. P. G. Luo, S. Sahu, S. T. Yang, S. K. Sonkar, J. Wang, H. Wang, G. E. Lecroy, L. Cao and Y. P. Sun, *J. Mater. Chem. B*., **1**, 2116 (2013).
12. T. Boobalan, M. Sethupathi, N. Sengottuvelan, P. Kumar, P. Balaji, B. Gulyás, P. Padmanabhan, S. T. Selvan and A. Arun, *ACS Appl. Nano Mater*., **3**(6), 5910 (2020).
12. C. Yao, Y. Xu and Z. Xia, *J. Mater. Chem. C*, **6**, 4396 (2018).
13. H. Tetsuka, R. Asahi, A. Nagoya, K. Okamoto, I. Tajima, R. Ohta and A. Okamoto, *Adv. Mater*., **24**, 5333 (2012).
14. M. Chen, W. Wang and X. Wu, *J. Mater. Chem. B*, **2**, 3937 (2014).
15. P. K. Sarswat and M. L. Free, *Phys. Chem. Chem. Phys*., **17**, 27642 (2015).
16. S. Zhu, J. Zhang, S. Tang, C. Qiao, L. Wang, H. Wang, X. Liu, B. Li, Y. Li, W. Yu, X. Wang, H. Sun and B. Yang, *Adv. Funct. Mater*., **22**, 4732 (2012).
17. Y. Dong, R. Wang, H. Li, J. Shao, Y. Chi, X. Lin and G. Chen, *Carbon*, **50**, 2810 (2012).
18. T. J. Pillar-Little, N. Wanninayake, L. Nease, D. K. Heidary, E. C. Glazer and D. Y. Kim, *Carbon*, **140**, 616 (2018).
19. H. Qi, M. Teng, S. Liu, J. Li, H. Yu, C. Teng, Z. Huang, H. Liu, Q. Shao, A. Umar, T. Ding, Q. Gao and Z. Guo, *J. Colloid Interface Sci*., **539**, 332 (2019).
20. A. Boruah, M. Saikia, T. Das, R. L. Goswamee and B. K. Saikia, *J. Photochem. Photobiol. B: Biol*., **209**, 111940 (2020).
21. S. Ahmadian-Fard-Fini, M. Salavati-Niasari and D. Ghanbari, *Spectrochim. Acta A Mol. Biomol. Spectrosc*., **203**, 481 (2018).
22. Y. Kim, G. Jang and T. S. Lee, *ACS Appl. Mater. Interfaces*, **7**, 15649 (2015).
23. J. Li, O. Xu and X. Zhu, *RSC Adv*., **11**, 34107 (2021).
24. A. Ananthanarayanan, X. Wang, P. Routh, B. Sana, S. Lim, D. H. Kim, K. H. Lim, J. Li and P. Chen, *Adv. Funct. Mater*., **24**, 3021 (2014).
25. R. Sangubotla and J. Kim, *Appl. Surf. Sci*., **490**, 61 (2019).
26. S. R. Ankireddy, V. G. Vo, S. S. A. An and J. Kim, *ACS Appl. Bio Mater*., **3**, 4873 (2020).
27. N. Arumugam and J. Kim, *Mater. Lett*., **219**, 37 (2018).
28. S. Venkateswarlu, S. Govindaraju, R. Sangubotla, J. Kim, M. H. Lee and K. Yun, *J. Nanomater*., **9**, 245 (2019).
29. R. Sangubotla and J. Kim, *Mater. Sci. Eng. C*, **122**, 111916 (2021).
30. V. W. Y. Tam and C. M. Tam, *Resour. Conserv. Recycl*., **47**, 209 (2006).
31. M. Saberian, J. Li, A. Donnoli, E. Bonderenko, P. Oliva, B. Gill, S. Lockrey and R. Siddique, *J. Clean. Prod*., **289**, 125837 (2021).
32. C. K. Morikawa and M. Saigusa, *Plant Soil*, **304**, 249 (2008).
33. D. Pujol, C. Liu, J. Gominho, M. À. Olivella, N. Fiol, I. Villaescusa and H. Pereira, *Ind. Crops Prod*., **50**, 423 (2013).
34. B. Shi, Y. Su, L. Zhang, M. Huang, R. Liu and S. Zhao, *ACS Appl. Mater. Interfaces*, **8**, 10717 (2016).
35. S. M. Badawy, R. I. Liem, C. K. Rigsby, R. J. Labotka, R. A. DeFreitas and A. A. Thompson, *Br. J. Haematol*., **175**, 705 (2016).
36. T. H. Le, H. J. Lee, J. H. Kim and S. J. Park, *Sensors*, **20**(12), 3470 (2020).
37. R. Guo, S. Zhou, Y. Li, X. Li, L. Fan and N. H. Voelcker, *ACS Appl. Mater. Interfaces*, **7**, 23958 (2015).
38. G. P. Keeley, A. O'Neill, N. McEvoy, N. Peltekis, J. N. Coleman and G. S. Duesberg, *J. Mater. Chem*., **20**, 7864 (2010).
39. X. Wang, P. Wu, X. Hou and Y. Lv, *Analyst*, **138**, 229 (2013).
40. S. P. Sood, L. E. Sartori, D. P. Wittmer and W. G. Haney, *Anal. Chem*., **48**, 796 (1976).
41. A. Nag, A. Hazarika, K. V. Shanavas, S. M. Sharma, I. Dasgupta and D. D. Sarma, *J. Phys. Chem. Lett*., **2**, 706 (2011).
42. Q. H. Trinh, M. M. Hossain, S. H. Kim and Y. S. Mok, *Heliyon*, **4**, e00522 (2018).
43. Y.-S. Lin and C.-L. Chen, *J. Appl. Polym. Sci*., **110**, 2704 (2008).
44. H. Robberecht, K. Van Dyck, D. Bosscher and R. Van Cauwenbergh, *Int. J. Food Prop*., **11**, 638 (2008).
45. B. Sivaranjini, R. Mangaiyarkarasi, V. Ganesh and S. Umadevi, *Sci. Rep*., **8**, 1 (2018).
46. C. Kim, J. Lee, W. Wang and J. Fortner, *J. Nanomater*., **10**(6), 1228 (2020).
47. A. Morais, J. P. C. Alves, F. A. S. Lima, M. Lira-Cantu and A. F. Nogueira, *J. Photonics Energy*, **5**, 057408 (2015).

48. B. J. Matsoso, K. Ranganathan, B. K. Mutuma, T. Lerotholi, G. Jones and N. J. Coville, *New J. Chem.*, **41**, 9497 (2017).
49. R. Djara, Y. Holade, A. Merzouki, M. A. Lacour, N. Masquelez, V. Flaud, D. Cot, B. Rebiere, A. van der Lee, J. Cambedouzou, P. Huguet, S. Tingry and D. Cornu, *Front. Chem.*, **8**, 385 (2020).
50. C. Christodoulou, B. Wolter, A. Ioakeimidis, G. Chouliaras, S. Wiesner, I. Lauermann, A. Centeno, A. Zurutuza and K. Fostiropoulos, *Thin Solid Films*, **682**, 57 (2019).
51. K. M. Omer, *Anal. Bioanal. Chem.*, **410**, 6331 (2018).
52. Z. Xing, Z. Ju, Y. Zhao, J. Wan, Y. Zhu, Y. Qiang and Y. Qian, *Sci. Rep.*, **6**, 1 (2016).
53. D. Fang, F. He, J. Xie and L. Xue, *J. Wuhan Univ. Technol. Mater. Sci. Ed.*, **35**, 711 (2020).
54. S. Akyuz, T. Akyuz, O. Celik and C. Atak, *J. Mol. Struct.*, **1044**, 67 (2013).
55. G. Premaratne, S. Farias and S. Krishnan, *Anal. Chim. Acta*, **970**, 23 (2017).
56. S. Sean, Q. A. Binh, D. Tungtakanpoung and P. Kajityichyanukul, *IOP Conf. Ser. Mater. Sci. Eng.*, **617**, 012012 (2019).
57. S. P. Ashby, J. A. Thomas, J. García-Cañadas, G. Min, J. Corps, A. V. Powell, H. Xu, W. Shen and Y. Chao, *Faraday Discuss.*, **176**, 349 (2014).
58. Q. Chen, K. Zhou, Y. Chen, A. Wang and F. Liu, *RSC Adv.*, **7**(21), 12812 (2017).
59. J. J. Senkevich, C. J. Mitchell, G. R. Yang and T. M. Lu, *Langmuir*, **18**, 1587 (2002).
60. L. Zhang, L. Y. Tu, Y. Liang, Q. Chen, Z. S. Li, C. H. Li, Z. H. Wang and W. Li, *RSC Adv.*, **8**(74), 42280 (2018).
61. A. Šarić, S. Musić, K. Nomura and S. Popović, *Mater. Sci. Eng. B*, **56**, 43 (1998).
62. N. Puvvada, B. N. P. Kumar, S. Konar, H. Kalita, M. Mandal and A. Pathak, *Sci. Technol. Adv. Mater.*, **13**, 045008 (2012).
63. A. F. Shaikh, M. S. Tamboli, R. H. Patil, A. Bhan, J. D. Ambekar and B. B. Kale, *J. Nanosci.*, **19**, 2339 (2019).
64. J. Zhang, W. Shen, D. Pan, Z. Zhang, Y. Fang and M. Wu, *New J. Chem.*, **34**, 591 (2010).
65. V. Raveendran, A. R. Suresh Babu and N. K. Renuka, *RSC Adv.*, **9**(21), 12070 (2019).
66. S. R. Ankireddy and J. Kim, *Sens. Actuators B Chem.*, **255**, 3425 (2018).
67. Y. Kim and J. Kim, *Opt. Mater. (Amst)*, **99**, 109514 (2020).
68. M. E. K. Wahba, N. El-Enany and F. Belal, *Anal. Methods*, **7**, 10445 (2015).
69. G. L. Wang, Y. M. Dong and Z. J. Li, *Nanotechnology*, **22**, 085503 (2011).
70. X. Gao, X. Zhou, Y. Ma, T. Qian, C. Wang and F. Chu, *Appl. Surf. Sci.*, **469**, 911 (2019).
71. X. Luo, W. Zhang, Y. Han, X. Chen, L. Zhu, W. Tang, J. Wang, T. Yue and Z. Li, *Food Chem.*, **258**, 214 (2018).
72. X. Ma, S. Lin, Y. Dang, Y. Dai, X. Zhang and F. Xia, *Anal. Bioanal. Chem.*, **411**, 6645 (2019).
73. P. Zhao, K. He, Y. Han, Z. Zhang, M. Yu, H. Wang, Y. Huang, Z. Nie and S. Yao, *Anal. Chem.*, **87**, 9998 (2015).
74. G. Hu, L. Ge, Y. Li, M. Mukhtar, B. Shen, D. Yang and J. Li, *J. Colloid Interface Sci.*, **579**, 96 (2020).